Visualization of Doppler Radar Data
Three-Dimensional Images of Snow Bands

Masayuki MAKI   and Hideo MIYACHI

Advanced Technology Research Group
National Research Institute for Earth Science and Disaster Prevention, Japan
maki@bosai.go.jp
KGT Inc., Japan
miyachi@kubota.co.jp

Abstract

Three-dimensional computer graphic techniques are applied to the processing of snowstorm radar data. The following techniques are examined: 1) perspective representation of radar data; 2) zooming; 3) change in viewing angle and viewing point; 4) arbitrary cross-sectional analysis; and 5) time sequence analysis of perspective images.

Perspective representation of radar data enables us to interpret radar echoes more effectively and more intuitively. The man-machine interactive processing abilities of 3DCG such as zooming, changing the viewing angle and making arbitrary cross-sections are useful for the analysis of radar data. Time sequence analysis of perspective images of the radar data is especially useful in revealing the generation, development and decay processes of snowstorms, which are four-dimensional, and important items which are sometimes overlooked by conventional two-dimensional representation. This type of display can be called the Three-Dimensional Indicator (TDI), following the naming pattern of the Plan Position Indicator (PPI) and Range Height Indicator (RHI).

Key words : Doppler radar, Visualization, Snow band, Computer graphics

1.   Introduction

An indicator is one of the components of a weather radar system. It presents radar data in observable form and provides useful meteorological information about the targets. In the early development stage of weather radars during and after World War II, cathode-ray tubes (CRTs) were commonly used as indicators. A weather echo was shown as a luminous spot on the dark face of a CRT. This type of indicator could provide only semi-quantitative photographic data. After digitization of radar data became possible in the 1970s, color CRT monitors became the most commonly used indicator devices, since they can display quantitative data more efficiently. The importance of indicators in radar systems is increasing, since they are essential both as monitors of weather phenomena and as tools for data analysis.

Radar indicators can be classified into three types according to the spatial dimensions of the radar echo images. The simplest indicator is a one-dimensional display. A typical example of this kind of display is a type A display or A-scope which displays received signals on an oscilloscope screen with the amplitude of the signals represented as a function of range. A-scopes are still commonly used for testing radar systems and for setting the optimal azimuth and elevation angles.

The second type of display is a two-dimensional display. Examples are the Plan Position Indicator (PPI), Range Height Indicator (RHI) and Constant Altitude Plan Position Indicator (CAPPI). In a PPI, the radar echo signals are shown in plan for with the range and azimuth angle displayed as polar coordinates. In an RHI, data is

Tennodai 3-1, Tsukuba, Ibaraki, 305-0006, Japan

Shinjuku 2-8-8, Shinjyuku-ku, Tokyo, 160-0022, Japan

presented on a CRT screen with height as the vertical axis and the range as the horizontal axis. In a CAPPI, the radar echo at a constant altitude is shown as a plan figure.

Though these types of displays are useful in representing radar echoes, difficulties are sometimes encountered when we interpret them. One of the main reasons for these difficulties is that conventional display methods are restricted to two-dimensional representation with a time component, while meteorological phenomena are essentially three-dimensional with a time component. To gain a clearer and more effective understanding of radar echoes, three-dimensional representation, the third type of display, has been proposed by several researchers (e.g., Hibbard 1986, Papathomas *et al*. 1988). The recent progress of three-dimensional computer graphics (3DCG) has encouraged the application of this type of representation as a tool for data analysis and as a monitor for radar systems. The hardware and software for 3DCG are now commercially available, and have the power and variety of features needed to process high volumes of observed data. The purpose of the present paper is to demonstrate the effectiveness of three-dimensional visualization of weather radar data. A detailed discussion of the structure and formation mechanism of snow bands is beyond the scope of this report.

2. Brief review of three-dimensional representation of radar data

Application of three-dimensional data representation techniques in meteorology probably started in the late 1980s. Pioneering work on time sequence analysis of three-dimensional perspective images was proposed and examined by Hibbard (1986). Papathomas *et al*. (1988) showed three-dimensional representation of a variety of meteorological data such as the results of numerical model calculation, satellite data and ground-based weather data.

Several methods of three-dimensional representation have been proposed. The simplest method is to show a three-dimensional structure by arranging two-dimensional images. Examples of this method are those of Sarreals *et al*. (1986), Nakakita *et al*. (1988), and Dunn (1990). They applied this method to radar reflectivity data and showed the three-dimensional structures of precipitation systems by arranging CAPPI images with different heights and RHI images with different azimuth angles. The wire-frame perspective display technique is also a well-known method. Grotjahn and Chervin (1984) efficiently used this method to show model-generated data. Vonder Haar *et al*. (1988) also applied this method to the combination of

satellite and radar data.

A more sophisticated and realistic display method is the three-dimensional perspective technique which uses illumination and shading algorithms. Hasler *et al*. (1985) applied this technique to visible and infrared images of hurricanes. Fujiyoshi *et al*. (1991) visualized radar reflectivity data more realistically and investigated the inner structure of precipitating systems by creating horizontal and vertical cross-sections. In addition to radar reflectivity, Maki *et al*. (1992) visualized Doppler velocity and spectrum width data.

3. Data and three-dimensional computer graphics
3.1 Data

The data used in the present study are Doppler radar data of snowstorms observed above the Tsugaru Plain in the northern part of Japan's main island of Honshu. A rapid scanning Doppler radar provided by the National Research Institute for Earth Science and Disaster Prevention was used for the observations. The main specifications of the Doppler radar are listed in **Table 1**. The radar has a maximum antenna rotation speed of 15 rpm as well as a variety of antenna scanning modes. During a four-year period of observations of snowstorms (1989 to 1992), the NIED radar observed a typical snow band in 1990. Radar data for well-developed snow bands were acquired with good spatial and temporal resolution, providing a good case for studying the structure and time evolution of snowstorms by 3DCG. The spatial resolution of the data is about 1º in azimuth angle and 250 m in range direction. The volume data, which consists of 19 PPI scans with elevation angles from 0.6º to 21.6º, were acquired every 6 minutes. The time required to obtain volume scan data was about 4 minutes. Three kinds of radar data (reflectivity, Doppler velocity and spectrum width) were obtained.

3.2 Coordinate transformation

Radar data on PPI and RHI are generally acquired on a polar coordinate system. It is more convenient, however,

Table 1 Characteristics of the NIED Doppler radar.

Wavelength (cm)	3.2
Peak power (kW)	40
PRF (Hz)	2000
Pulse width (μ s)	0.5
Beamwidth (°)	1.2
Antenna diameter (m)	2
Antenna gain (dB)	42
Antenna Rotation rate (rpm)	15 (max)
Minimum detectable signal (dBm)	-105

to deal with radar data on a Cartesian coordinate system. There are several schemes for the coordinate transformation of radar data; the nearest-neighbor method, by which radar data on a polar coordinate grid point is transformed on its nearest grid point to a Cartesian coordinate system, or the simple or weighted average method by which radar data within spheres surrounding each Cartesian grid point are averaged. In this paper, the nearest-neighbor method was adopted since it uses a simple algorithm and thus features the shortest calculation time for data transformation. Storm advection during the time period of one volume scan is not considered in the present study. Thus, some distortion of echo structure may be present.

Computation for the image data processing was done for each of the grid points on a 321 x 321 x 16 array. The resolution of the array is 250 m in both the horizontal and vertical directions.

3.3 Three-dimensional computer graphics software

The software was Application Visualization System 3 (AVS3) which was designed and programmed by AVS Inc. for the visualization of scientific data. The following functions of this 3DCG software were examined:

1) Perspective representation with illumination and shading techniques;
2) Zoomability;
3) Change of viewing angle and viewing point;
4) Arbitrary cross-section scanning; and
5) Configuration of the time sequences of three-dimensional images.

4.   Results

4.1   Perspective view

A perspective view of the snow band is shown in **Fig. 1 (a)**. The 13 dBZ isosurface, which corresponds to a rainfall rate of about 0.1 mm/h, is visualized by illumination and shading techniques. To gain information on the dependence of echo evolution on the topography, we represented the topography of the Tsugaru area by using altitude data provided by the Geographical Survey Institute of the Ministry of Construction, Japan. To investigate the shape of the snow band, we changed the viewing angle. The zooming view from the direction indicated by the white arrow in **Fig. 1 (a)** is shown in **Fig. 1 (b)**. The side and top views of the snow band are shown in **Fig. 1 (c)** and **(d)**, respectively. The snow band has a width of about 15 km and an orientation from the southwest to the northeast. The echo top of the snow band is about 3 km. The snow band aspect ratio, defined by the ratio of horizontal distance between two bands and the vertical extent, is

about 10. This value is larger than the values predicted from laboratory experiments and numerical models. This means that observed snow bands have a flatter shape than that expected from theoretical studies. The geometrical characteristics of observed snow bands in the present study are similar to those for horizontal roll convection observed by Christian and Wakimoto (1989).

From **Fig. 1 (b)** and **(d)**, it is clear that the snow band is composed of meso- scale convective echo cells arranged in the band orientation. This feature of snow bands was also found by Fujiyoshi *et al.* (1998).

4.2   Arbitrary cross-section scanning

Arbitrary cross-sectional analysis is one of the advantages provided by 3DCG software functions. It enables us to investigate the inner structure of snow bands. Examples of the horizontal and vertical cross-sections are shown in **Fig. 2** and **Fig. 3**, respectively. To diagnose the inner structure of the snow band, the horizontal and vertical cross-sections were moved. The white arrows in **Fig. 2 (d)** and **Fig. 3 (d)** indicate the directions of the cross-sectional motions. The series of images were saved on a disk and recorded on a CD-ROM (**Movies 1**, **2** and **3**; see Appendix) to allow them to be investigated repeatedly. This type of analysis is similar to the computer tomography scans (CT scans) which are commonly used in diagnostic medicine. From the cross-section scanning analysis it was found that echo cells of the snow band had snowfall cores in their center. The maximum radar reflectivity factor is about 30 dBZ. The lifetime of most composite echo cells was about 1 hour, which was longer than that of non-organized convective echo cells. The wind structure inside the snow bands could also be seen; Doppler velocities rose to high levels over the Tsugaru Mountains.

The time required to make a cross-section, which is dependent on computer power, is crucial for cross-section scanning analysis. However, real-time cross-sectional analysis has been enabled by recent developments in computing techniques.

4.3   Time sequence of perspective echo images

Volume scan data obtained every 6 minutes over a period of about 7 hours were processed. The created images were saved to disk and a CD-ROM. Playback of the animated images shows clear changes over time in the snow band orientation. Four images chosen from the time sequence images are shown in **Fig. 4**. Band orientation angles measured with respect to the geostrophic wind direction at 11:57 LST, 13:30 LST, and 16:25 LST are -19º, -30º, and 13º, respectively. It can be seen that there are two different orientations at 11:57 LST; one is the snow band itself and the other is the orientation of the composite echo cells of the snow band.

At 14:58 LST it was difficult to define the band orientation.

As shown in **Movie 4**, snow bands did not remain in a steady state. Since a snow band can be classified as a horizontal vortex in the atmospheric boundary layer flow, changes in the band geometry appear to be related to changes in the instability mechanisms of horizontal vortices. Three types of instability mechanisms have been proposed to explain the geometry of horizontal vortices (e.g. Etling and Brown, 1993); inflection point instability, parallel instability, and thermal instability. Although these instability mechanisms can explain the basic features of snow bands, there is a discrepancy in the band orientation and the aspect ratio between the theoretical values and the observed values. Generally, the observed band orientation shows more variability than the theoretically expected values. The observed aspect ratio of snow bands also differs from the theoretical values: the observed band has a flatter shape. One of the reasons for this discrepancy is the effect of release of latent heat. The interaction between meso-scale convective clouds within a snow band (Fujiyoshi *et al*., 1998) may affect snow band geometry. Recently, Yoshimoto *et al*. (2000) showed that the outflow from meso- scale echoes of a snow band intensified the adjacent snow band. The interaction between two adjacent snow bands may also affect the geometrical character of snow bands.

Another interesting feature is the modification of snow bands by mountains. The radar echoes are weakened behind Mt. Iwaki, which is a conical mountain with a height of 1800 m, located south of the Tsugaru area. The modification of snow echoes over the Tsugaru Mountains was shown by Kodama *et al*. (1999).

One of the advantages of the time sequence analysis of the perspective images is that we can know at what height the echo cell was generated and dissipated. One of the interesting findings from the time sequence analysis of snow bands is the generation of an arc-shaped echo, indicated by the white arrow in **Fig. 5** (also see **Movie 5**). The echo intensity is weak, and the echo top height defined by 13 dBZ reflectivity was below 1000 m. Its lifetime was shorter than 15 minutes. The record of an ultrasonic anemometer-thermometer showed a gust of 15 m/s and an air temperature drop of 0.5 at 18:22 LST when the arc-shaped echo passed over the radar site. The Doppler velocity pattern also suggested the presence of a gust front along this echo. These pieces of observational evidence suggest that the generation of the arc-shaped echo was related to the cold outflow from the snow band. It is well known that dust storms are generated by thunderstorm-induced gusts. When a

downdraft from a well-developed cumulonimbus reaches the surface, it diverges and moves as a cold outflow, generating a gust front. Wakimoto (1982) analyzed thunderstorm outflows at different stages and found that a "precipitation roll" is formed in the leading outflow at the decay stage when the gust front advances ahead of the squall line. In the case of snowstorms, although the strength of the downdraft and cold air outflow may be weaker than that seen in thunderstorms (e.g. Maki and Nakamura, 1995), similar processes are likely to take place.

Our analysis of snowstorms also showed multiple surge-like echoes, which are one of the characteristics of a thunderstorm outflow (**Fig. 6** and **Movie 6**).

5. Summary

As mentioned by Sauvageot (1992), a modern weather radar system comprises two components, a captor and a computer. Recent advances in computer technology, increases in speed and capacity, and falling costs make it possible to represent three-dimensional images on a color monitor. In the present study, a commercially available 3DCG software package was applied to the processing of snowstorm radar data. The structure of snow bands is clearly shown by the perspective representation, zooming and arbitrary cross-sectional analysis of radar data. The change of snow band orientation and generation of echoes associated with snowstorm-induced gusts are found from the time sequence analysis of three-dimensional images. The time sequence analysis is especially useful for gaining information on important details of generation, development and decay processes of severe storms which are sometimes overlooked in conventional two-dimensional representations. This new type of display method can be called the Three-Dimensional Indicator (TDI), corresponding to the naming pattern of PPI and RHI.

There may be some problems when applying the TDI method to conventional Doppler radars which have a slow antenna scanning speed. In the present study, we used the rapid scanning Doppler radar to reduce the problems mentioned below. Due to slow antenna scanning, an observation time difference in the volume data will occur at each scan. It is thus necessary to correct the advection of a radar echo during a volume scan period to construct a three-dimensional image. Without this advection correction, some distortion may occur in the three-dimensional radar image, particularly for echoes located near the radar site or echoes with high echo tops. The second form or distortion is artificial ring patterns which are due to the combined effects of the limitation of total scan number in a volume scan data and
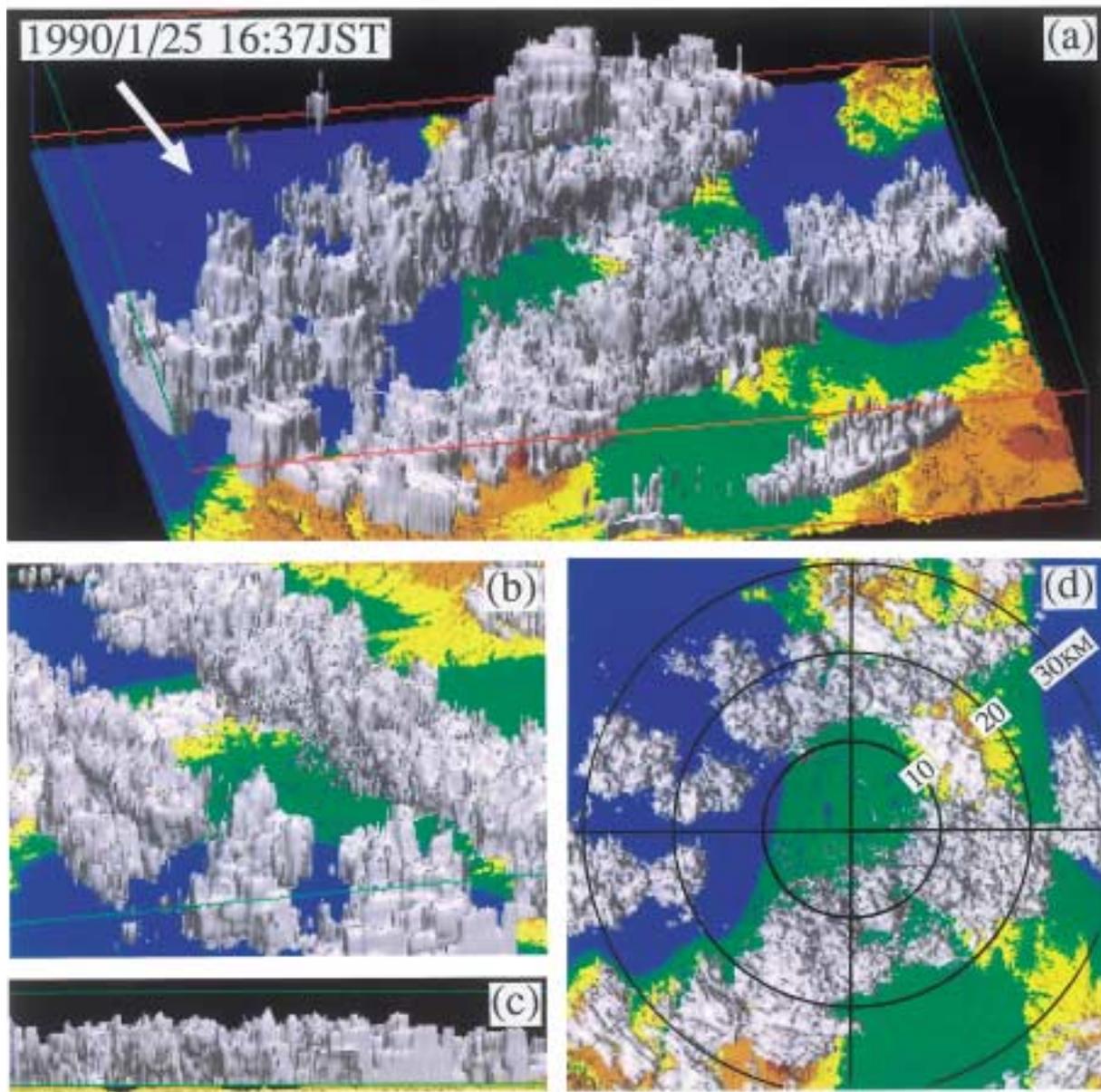
Fig. 1 Three-dimensional representation of the snow band superimposed on the topography. (a) Perspective view, (b) zooming view, (c) side view, and (d) top view. The blue, green, yellow, light brown, and dark brown areas show the sea surface, the area of altitude lower than 100 m, altitude from 100 m to 300 m, altitude from 300 m to 1000 m, and altitude higher than 1000 m, respectively. The actual size of the box is 80 km in width and length and 4 km in height. The vertical scale has been exaggerated by a factor of 3. The echoes on mountain areas are ground echoes.
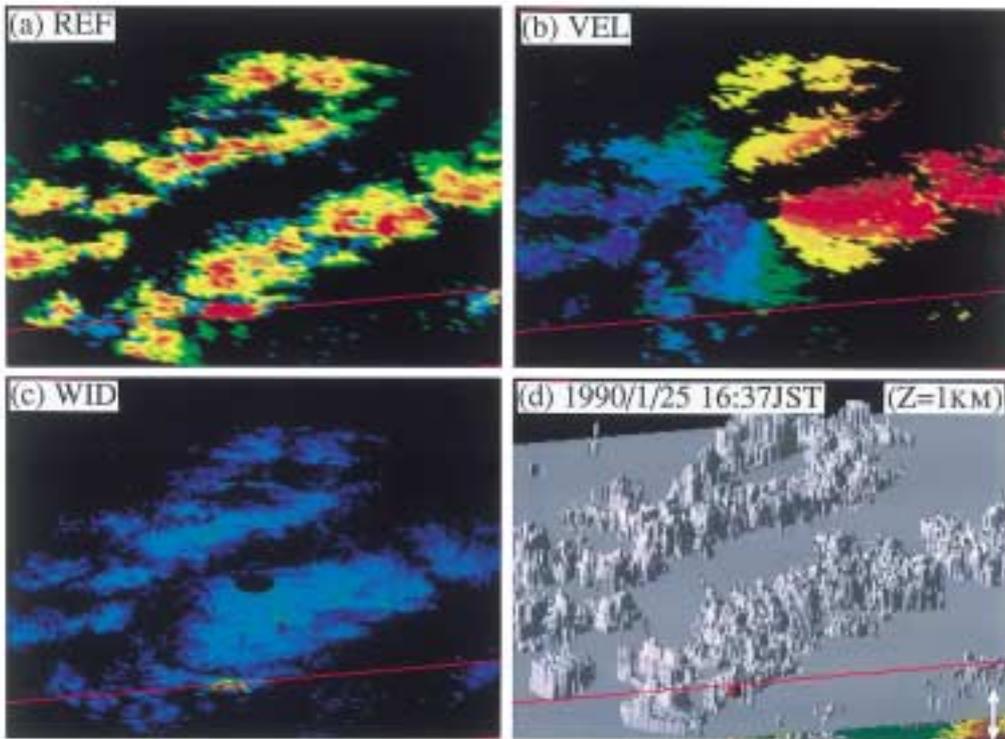
Fig. 2 Horizontal cross-section scanning of (a) reflectivity, (b) Doppler velocity, (c) spectrum width, and (d) position of the cross section. In the animated movies, the position of the cross section moves in the direction indicated by the white arrow.
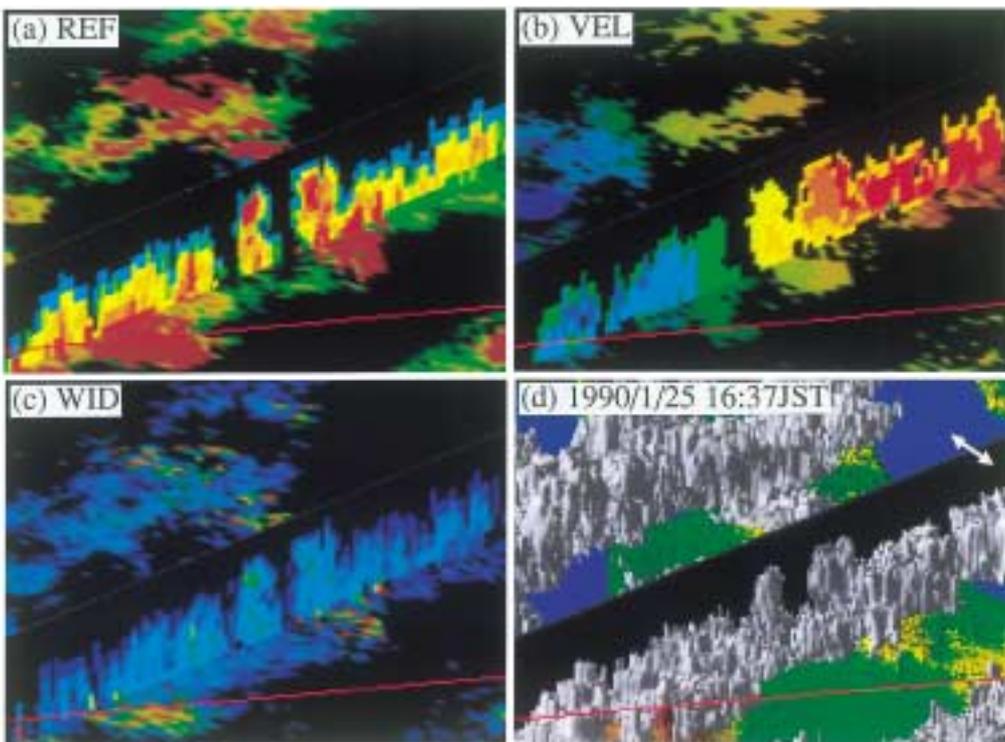
Fig. 3 Same as **Fig. 2** except for vertical cross-section scanning. Vertical cross-sections are superimposed on the horizontal cross-section at the height of 250 m. In the animated movies, the position of the cross-section moves in the direction in dicated by the white arrow.
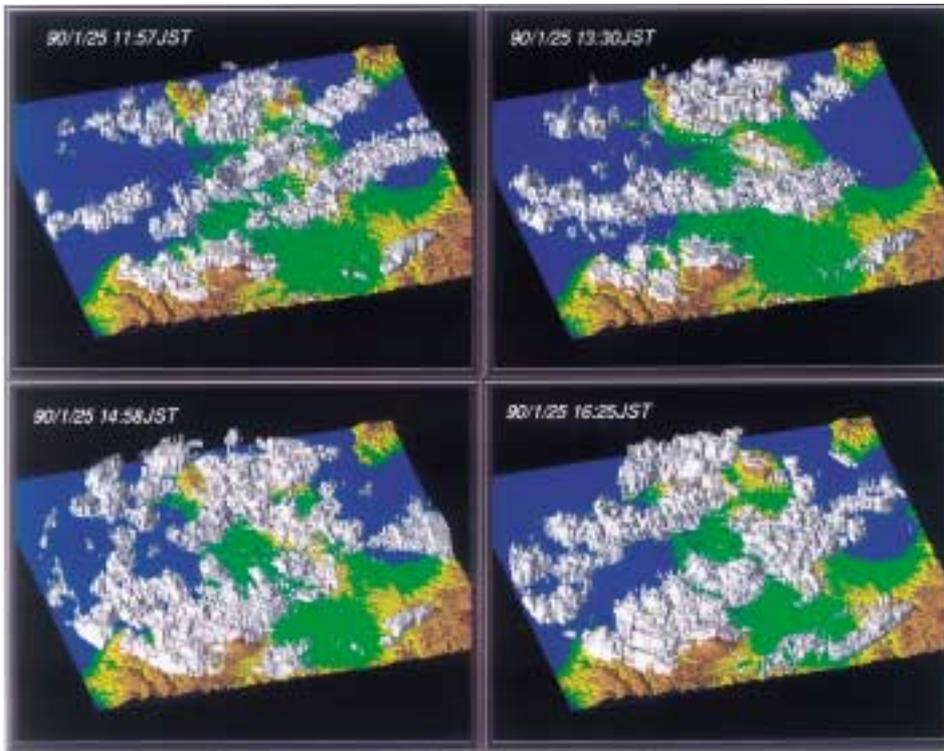
Fig. 4 Time sequence of oblique views showing the changes in the snow band organization.
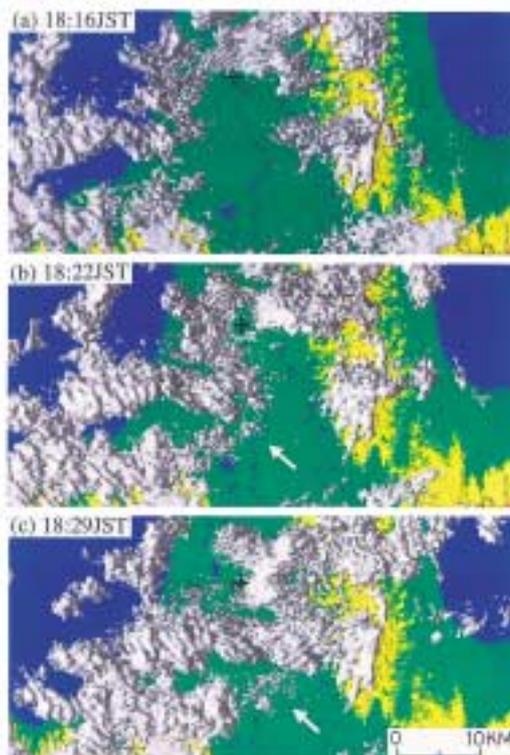
Fig. 5 Time sequence of top views of a "precipitation roll"-like echo which is indicated by a white arrow and may be generated by the cold outflow from the snow band. The radar site is shown by "+".
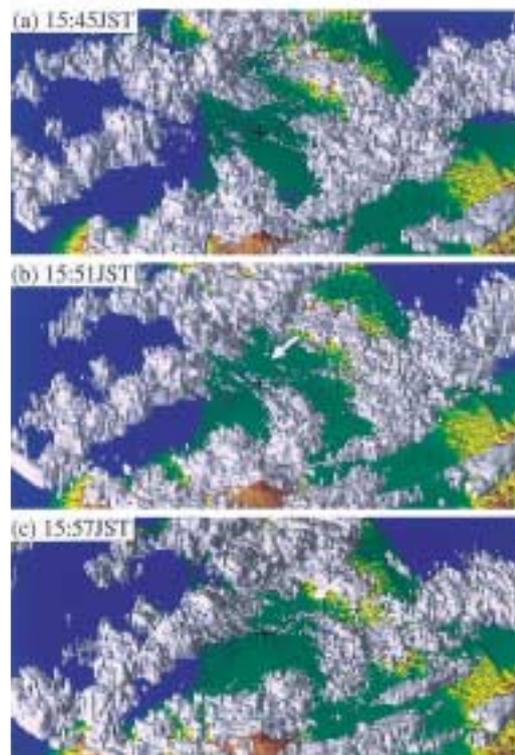
Fig. 6 Time sequence of oblique views of multiple surge-like echoes indicated by a white arrow. The radar site is shown by "+".

the increase in beam width with the range. Results shown in the present paper were obtained using the advantages of rapid scanning Doppler radar, thus reducing the effects of above-mentioned problems.

With the development of polarimetric radar technology, TDI can be applicable to microphysical classification. Information on microphysical parameters such as hydrometeor type and their size distribution estimated from polarimetric radar measurements can be effectively shown by TDI. Arbitrary cross-sectional analysis will be useful not only for practical purposes such as the detection of hail regions but also for gaining a fuller understanding of microphysical processes.

Appendix

Animated radar images

The CD-ROM containing the following movies will be available from the National Research Institute for Earth Science and Disaster Prevention. The CD-ROM contains the following movies. Since the images are in the form of animated GIF files, they are viewable using a standard internet browser or by any suitable viewing software. The original images were divided into 4 images in **Movies 1**, **2**, and **3** because of limitations of memory and the speed of PCs.

Movie 1

Horizontal cross-section scanning of snow bands: (a) radar reflectivity, (b) Doppler velocity, (c) spectrum width, and (d) 13 dBZ iso-surface.

Movie 2

Vertical cross-section scanning of snow bands: (a) radar reflectivity, (b) Doppler velocity, (c) spectrum width, and (d) 13 dBZ iso-surface. The vertical cross-section moves parallel to and perpendicular to band orientation.

Movie 3

Vertical cross-section scanning of snow bands: (a) radar reflectivity, (b) Doppler velocity, (c) spectrum width, and (d) 13 dBZ iso-surface. The vertical cross-section rotates around the vertical axis at the radar.

Movie 4

Time sequence of snow bands. (a) Oblique view. (b) Top view.

Movie 5

Generation of "precipitation roll" (Wakimoto, 1982) associated with snowstorm outflows.

Movie 6

Multiple surge-like echoes.

References

1) Christian, T.W., and R.M. Wakimoto (1989) The relationship between radar reflectivities and clouds associated with horizontal roll convection on 8 August 1982. Mon. Wea. Rev., **117**, 1530-1544.

2) Dunn, L.B. (1990) Two examples of operational tornado warning using Doppler radar data. Bull. Amer. Meteor. Soc., **71**, 145-153.

3) Etling, D., and R. A. Brown (1993) Roll vortices in the planetary boundary layer: A review, Bound.-Layer Meteor., **65**, 215-248.

4) Fujiyoshi, Y., M. Ohi, and G. Wakahama (1991) Three-dimensional display of radar echoes using the technique of marching cubes. J. Atmos. Oceanic Technol., **8**, 869-872.

5) Fujiyoshi, Y., N. Yoshimoto, and T. Takeda (1998) A dual-Doppler radar study of longitudinal-meso snowbands. Part I: A three-dimensional kinematic structure of meso-scale convective cloud systems within a longitudinal-mode snowband. Mon. Wea. Rev., **126**, 72-91.

6) Grotjahn, R., and R.M. Chervin (1984) Animated graphics in meteorological research and presentations. Bull. Amer. Meteor. Soc., **65**, 1201-1208.

7) Hasler, A.F., H. Pierce, K.R. Morris, and J. Dodge (1985) Meteorological data fields "in perspective". Bull. Amer. Meteor. Soc., **66**, 795-801.

8) Hibbard, W.L. (1986) Computer-generated imagery for 4-D meteorological data. Bull. Amer. Meteor. Soc., **67**, 1362-1369.

9) Kodama, Y., M. Maki, S. Ando, M. Otsuki, O. Inaba, J. Inoue, N. Koshimae, S. Nakai, and T. Yagi (1999) A weak-wind zone accompanied with swelled snow clouds in the upstream of a low-altitude ridge   Single Doppler radar observations over the Tsugaru district of Japan   . J. Meteor. Soc. Japan, **77**, 1039-1059.

10) Maki, M., H. Ohkura, and T. Mikoshiba (1992) Applications of 3 dimensional computer graphics to the Doppler radar data processing. Rep. Natl. Res. Inst. Earth Sci. Disast. Prev., No. **49**, 53-64.

11) Maki, M., and H. Nakamura (1995) Doppler radar observations of snowstorm-induced strong winds. Preprints, 27th Conf. on Radar Meteor. Vail, Colorado, Amer. Meteor. Soc., Vail, 418-420.

12) Nakakita, E., M. Shiiba, S. Ikebuchi, and T. Takasao (1988) Visualization of the information from a three-dimensionally scanning radar raingauge. Proc. JSCE, **393**/ II-9, 161-169.

13) Papathomas, T.V., J.A. Schiavone, and B. Julesz (1988) Applications of computer graphics to the visualization of meteorological data. Computer Graphics, **22**, 327-334.

14) Sauvageot, H. (1992) Radar Meteorology, Artech

House, 366pp.

15) Sarreals, E.D., F. Toepfer, and J. Golden (1986) NEXRAD products and algorithms. part I: description and scientific basis. Preprints, Joint sessions, 23rd Conf. Radar Meteor. and Conf. Cloud Physics, Amer. Meteor. Soc., Boston, 83-87.

16) Vonder Haar, T.H., A.C. Meade, R.J. Craig, and D.L. Reinke (1988) Four-dimensional imaging for meteorological applications. J. Atmos. Oceanic Technol., **5**, 136-143.

17) Wakimoto, R.M. (1982) The life cycle of thunderstorm gust fronts as viewed with Doppler radar and rawinsonde data. Mon. Wea. Rev., **110**, 1060-1082.

18) Yoshimoto, N., Y. Fujiyoshi, and T. Takeda (2000) A dual-Doppler radar study of longitudinal-meso snowbands. Part II: Influence of the kinematics of a longitudinal-mode snowband on the development of an adjacent snowband. J. Meteor. Soc. Japan, **4**, 381-403.

3

3

3   2   3   4   5 3

1   3

2   3 3

4

Plan Position Indicator   PPI   Range Height Indicator   RHI

Three-Dimensional Indicator   TDI